

# Physical Emission of Spatially-Modulated Radar

**SHANNON D. BLUNT**<sup>1</sup>

University of Kansas

**PATRICK MCCORMICK**<sup>2</sup>

University of Kansas

**THOMAS HIGGINS**<sup>3</sup>

US Naval Research Laboratory

**MURALIDHAR RANGASWAMY**<sup>4</sup>

US Air Force Research Laboratory

Leveraging the recent development of a physical implementation of arbitrary polyphase codes as spectrally well-contained waveforms, the notion of spatial modulation is developed whereby a time-varying beam pattern is incorporated into the physical emission of an individual pulse. This subset of the broad category of MIMO radar is inspired by the operation of fixational eye movement within the human eye to enhance visual acuity and also subsumes the notion of the frequency-diverse array for application to pulsed radar. From this spatial modulation framework some specific emission examples are evaluated in terms of resolution and sidelobe levels for the delay and angle domains. The impact of spatial modulation upon spectral content is also considered and possible joint delay-angle emission design criteria are suggested. Simulation results of selected target arrangements demonstrate the promise of enhanced discrimination and the basis for the development of future cognitive radar capabilities that may mimic salient aspects of the visual cortex.

<sup>1</sup>Electrical Engineering & Computer Science Dept., 2335 Irving Hill Road, Lawrence, KS, 66045, [sdblunt@ittc.ku.edu](mailto:sdblunt@ittc.ku.edu).

<sup>2</sup>Electrical Engineering & Computer Science Dept., 2335 Irving Hill Road, Lawrence, KS, 66045, [patrick.m.mcc@gmail.com](mailto:patrick.m.mcc@gmail.com).

<sup>3</sup>Radar Division, Building 60, 4555 Overlook Ave. SW, Washington, DC, 20375, [Thomas.Higgins@nrl.navy.mil](mailto:Thomas.Higgins@nrl.navy.mil).

<sup>4</sup>Sensors Directorate, Building 620, 2241 Avionics Circle, Wright-Patterson AFB, OH, 45433, [muralidhar.rangaswamy@us.af.mil](mailto:muralidhar.rangaswamy@us.af.mil).

This work was supported in part by the Air Force Office of Scientific Research, the Naval Research Laboratory – Radar Division, and the Office of Naval Research base funding program. All views and opinions expressed here are the authors' own and do not reflect the official position of the U.S. Department of Defense.

Portions of this paper were presented at the 2014 IEEE Radar Conference [1].

## I. INTRODUCTION

Traditionally, electronically scanned radar systems emit a waveform-modulated pulse in a single spatial direction by applying a fixed inter-element phase shift across the antenna array, with an otherwise identical waveform being generated by each of the antenna elements. The received echoes are thus likewise characterized by the same waveform response regardless of spatial direction. In contrast, the notion of transmitting different, albeit correlated, waveforms from the elements of an array has been proposed [2-12] as a method to broaden the transmit beamwidth (i.e. beam-spoiling) for the purpose of achieving, for example, simultaneous multi-mode radar [12-15].

Here we consider the specific case in which the pulsed radar emission possesses both a temporal modulation (the waveform) and an *intra*-pulse spatial modulation that can be viewed as a form of fast-time time-division beamforming [5-12], a prominent example of which is the frequency-diverse array concept [5-10]. The proposed spatial modulation scheme actually subsumes this frequency-diverse array concept within the framework of pulsed emissions.

There is an interesting biological analog to this proposed scheme found in the visual system of humans and other animals possessing fovea in which the particular direction of attention is spatially modulated in a seemingly random manner (Fig. 1) via slow movements known as *drift* and rapid movements known as *microsaccades* [1,16,17]. While the purpose of these *fixational eye movements* has long been debated and remains an open research topic, the current consensus is that these small, spatial perturbations improve visual acuity because the associated transients enhance contrast and sensitivity as well as aiding in the resolving of spatial ambiguities. Furthermore, there is evidence [18] that these eye movements adapt according to environmental conditions (e.g. amount of lighting) and the active attention of the observer thereby suggesting a linkage between the physical actuation of the (passive) sensor and higher-level cognition, which for the extension here to active sensing implies an application within the context of cognitive radar [19].

With this visual/neurological antecedent as a source of inspiration, we consider the concept of fast-time spatial modulation of a pulsed emission by employing an inter-element phase shift across the array

that varies over the duration of the pulsewidth. This emission strategy forms a subset of the more general class of multiple-input multiple-output (MIMO) radar transmit schemes. Here, an approach denoted as the waveform diverse array (WDA) is used to allow for selection and physical generation of an arbitrary FM-based waveform while also providing control over the fast-time-dependent spatial beampattern during the pulse. The characteristics of the WDA approach are assessed relative to the traditional beamformed emission by examining the time-varying beampattern, aggregate beampattern, and an ambiguity function that is dependent on delay, transmit spatial angle, and receive spatial angle. A framework for determining the impact of spatial modulation on spectral content is also developed.

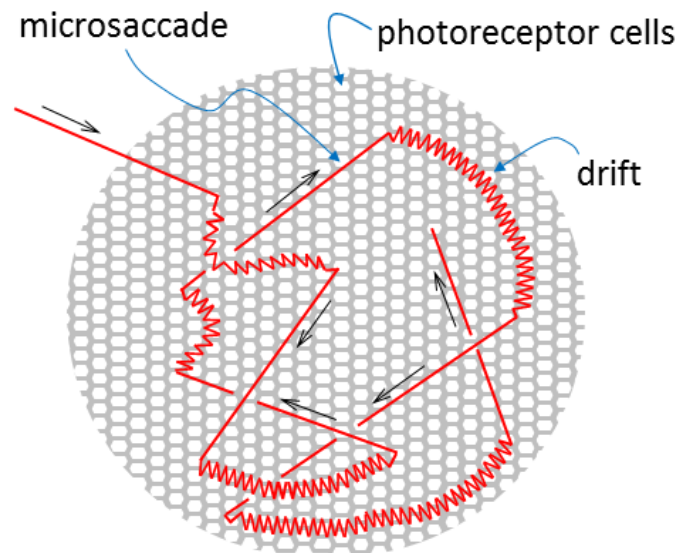


**Figure 1** Example of small eye movements during fixation

The diversity afforded by this spatially-modulated emission strategy is achieved by coupling the spatial angle and delay (range) domains and is conceptually similar to the angle-Doppler coupling of clutter that occurs for ground moving target indication (GMTI) from an airborne/space-based platform, for which the development of space-time adaptive processing (STAP) was necessitated. It is demonstrated that the interaction between the waveform and spatial modulation structures can produce joint emissions in which both delay and angle sidelobe reduction is achieved and spatial resolution is enhanced with only the use of angle-dependent receiver matched filtering (i.e. without adaptive receive processing).

The remainder of the paper is organized as follows. Section II introduces the WDA scheme for physical generation of spatially-modulated emissions, along with associated performance metrics, analysis of spectral content, and evaluation of some exemplary cases. In Section III simulation results are presented for different scattering scenarios with the various emission schemes to assess the impact of spatial modulation in the delay and angle domains and the diversity enhancement it affords for sensing. Section IV summarizes the observations of spatial modulation and discusses areas of ongoing/future work.

## II. WAVEFORM DIVERSE ARRAY (WDA)

The biological counterpart of fixational eye movement clearly suggests the use of a two-dimensional array (for spatial modulation in azimuth and elevation). While the WDA concept is applicable to any array geometry, for the sake of illustration we shall herein focus on the uniform linear array (ULA). The array element spacing is denoted as  $d$  with spatial angle  $\theta$  defined relative to array boresight (at which  $\theta = 0^\circ$ ). It is assumed that emitted/received signals satisfy the array narrowband assumption and thus the associated electrical phase angle is  $2\pi d \sin(\theta) / \lambda$ , with  $\lambda$  the wavelength of the carrier frequency.

### A. WDA Definition

The waveform diverse array (WDA) concept employs an independent waveform generator behind each element of the antenna array. To link the phase modulation of the waveform with the element-wise spatial modulation in fast-time we leverage the continuous phase modulation (CPM) framework described in [20,21] that generates polyphase-coded FM (PCFM) waveforms (Fig. 2). First, given a polyphase radar code with the  $N+1$  phase values  $\phi_0, \phi_1, \dots, \phi_N$ , a train of  $N$  impulses with time separation  $T_p$  are formed such that the total pulsewidth is  $T = NT_p$ . The  $n^{\text{th}}$  impulse is weighted by  $\alpha_n$ , which is the phase change between successive polyphase code values as determined by

$$\alpha_n = \begin{cases} \tilde{\alpha}_n & \text{if } |\tilde{\alpha}_n| \leq \pi \\ \tilde{\alpha}_n - 2\pi \operatorname{sgn}(\tilde{\alpha}_n) & \text{if } |\tilde{\alpha}_n| > \pi \end{cases}, \quad (1)$$

where

$$\tilde{\alpha}_n = \phi_n - \phi_{n-1} \quad \text{for } n=1, \dots, N, \quad (2)$$

and  $\text{sgn}(\bullet)$  is the signum operation. The shaping filter  $g(t)$  may, for example, be rectangular or raised cosine with the requirements 1) that it integrates to unity over the real line; and 2) that it has time support on  $[0, T_p]$ . The PCFM waveform is thus

$$s(t; \mathbf{x}_w) = \exp \left\{ j \left( \int_0^t g(\tau) * \left[ \sum_{n=1}^N \alpha_n \delta(\tau - (n-1)T_p) \right] d\tau + \phi_0 \right) \right\}, \quad (3)$$

where  $*$  denotes convolution,  $\phi_0$  is the initial phase value of the code, and the sequence of phase changes are collected into the vector  $\mathbf{x}_w = [\alpha_1 \ \alpha_2 \ \dots \ \alpha_N]^T$  which parameterizes the complex baseband waveform.

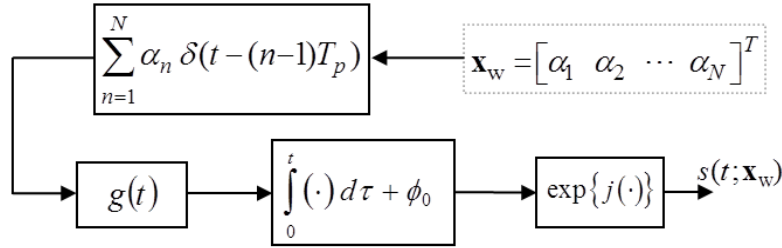


**Figure 2** CPM implementation to generate polyphase-coded FM (PCFM) waveforms

This framework can likewise be extended to parameterize in a physical manner the fast-time modulation of relative phase across the antenna array to facilitate spatial modulation during the pulse. Here a spatial modulation code comprised of  $N+1$  values  $\Delta_0, \Delta_1, \dots, \Delta_N$  is defined as a sequence of spatial angle offsets relative to some center direction  $\theta_C$ . The subsequent spatial phase-change sequence (as a function of code index  $n$ ) for use with the CPM implementation and a uniform linear array is thus

$$\varepsilon_n = \frac{2\pi d}{\lambda} \left( \sin(\theta_C + \Delta_n) - \sin(\theta_C + \Delta_{n-1}) \right) \quad \text{for } n=1, \dots, N, \quad (4)$$

noting that the values  $\Delta_n$  can be positive or negative and are small enough (when combined with  $\theta_C$ ) to avoid spatial “wrap around” beyond the endfire directions at  $\theta = \pm 90^\circ$ . Echoing the structure of (3), the spatial phase modulation as a function of continuous time is therefore

$$b(t; \mathbf{x}_s) = \exp \left\{ -j \left( \int_0^t g(\tau) * \left[ \sum_{n=1}^N \varepsilon_n \delta(\tau - (n-1)T_p) \right] d\tau + \bar{\Delta}_0 \right) \right\} \quad (5)$$

where the sequence of spatial phase changes are collected into the vector  $\mathbf{x}_s = [\varepsilon_1 \ \varepsilon_2 \ \cdots \ \varepsilon_N]^T$  and the initial electrical angle is

$$\bar{\Delta}_0 = \frac{2\pi d}{\lambda} \sin(\theta_C + \Delta_0). \quad (6)$$

The leading negative sign within the exponential of (5), relative to the waveform representation in (3), reflects the phase delay compensation for spatial beamsteering on transmit.

For the  $M$  antenna elements, define the half-wavelength-based position indexing as  $m = -0.5(M-1), -0.5(M-1)+1, \dots, +0.5(M-1)$  so that  $m=0$  is located at the center of the array, the indices are both positive and negative, and the indices increment by one. Note that when  $M$  is an even number, these indices will be offset by 1/2. This imposed symmetry is useful for physical intuition of the emission structure and is convenient for analysis of the impact on bandwidth for spatial modulation (Section II.C).

The signal generated by the antenna element with  $m^{\text{th}}$  position index is thus

$$s_m(t, \theta_C; \mathbf{x}_w, \mathbf{x}_s) = \frac{1}{\sqrt{T}} s(t; \mathbf{x}_w) b^m(t; \mathbf{x}_s), \quad (7)$$

where the normalization term provides unit transmit energy per antenna element and the Vandermonde-like form  $(\bullet)^m$  across the uniform linear array yields, from (7),

$$b^m(t; \mathbf{x}_s) = \exp \left\{ -jm \left( \int_0^t g(\tau) * \left[ \sum_{n=1}^N \varepsilon_n \delta(\tau - (n-1)T_p) \right] d\tau + \bar{\Delta}_0 \right) \right\}. \quad (8)$$

In the case of no spatial modulation, we have  $\Delta_0 = \Delta_1 = \cdots = \Delta_N = 0$  so that, from (4),  $\varepsilon_1 = \varepsilon_2 = \cdots = \varepsilon_N = 0$  likewise and (6) becomes  $\bar{\Delta}_0 = 2\pi d \sin(\theta_C) / \lambda$ . As a result, (8) simplifies to  $b^m(t; \mathbf{x}_s) = \exp\{-jm\bar{\Delta}_0\}$ , which is simply the phase delay on the  $m^{\text{th}}$  indexed antenna element needed to steer a stationary beam in the direction of spatial angle  $\theta_C$  (i.e. standard beamforming).

Finally, if we insert (3) and (8) into (7) the continuous CPM-implemented signal generated by the  $m^{\text{th}}$  indexed antenna element can be expressed as

$$s_m(t, \theta_C; \mathbf{x}_w, \mathbf{x}_s) = \frac{1}{\sqrt{T}} \exp \left\{ j \left( \int_0^t g(\tau) * \left[ \sum_{n=1}^N (\alpha_n - m\varepsilon_n) \delta(\tau - (n-1)T_p) \right] d\tau + (\phi_0 - m\bar{\Delta}_0) \right) \right\}. \quad (9)$$

In other words, defining for the  $m^{\text{th}}$  indexed antenna element a joint phase-change sequence  $\alpha_{n,m} = (\alpha_n - m\varepsilon_n)$  and initial phase  $\phi_{0,m} = (\phi_0 - m\bar{\Delta}_0)$ , the CPM radar implementation from Fig. 2 can be used with these values at each antenna element to produce the associated physical emission without needing an additional modulation stage in hardware.

It should also be noted that, as demonstrated by widespread use of CPM for applications such as aeronautical telemetry [22], deep space communications [23], and Bluetooth<sup>TM</sup> wireless [24], the radar-centric implementation in Fig. 2 is essentially a manifestation of FM that does not require the use of an arbitrary waveform generator (AWG), thereby avoiding the potentially high cost of deploying numerous AWGs for a MIMO radar to produce many different waveforms simultaneously. Furthermore, the emission scheme of (9) avoids the large phase differences between adjacent antenna elements that could otherwise cause radiation outside of real space which may damage the radar [25].

### B. WDA Beam pattern and Ambiguity Analysis

The WDA emission can be assessed by examining the time-varying beam pattern, aggregate beam pattern, and the angle-delay ambiguity function. These metrics are based on the normalized baseband representation of the composite far-field emission for time  $t$  and spatial angle  $\theta$  defined as

$$g(t, \theta, \theta_C) = \frac{1}{M} \sum_{m=-(M-1)/2}^{(M-1)/2} s_m(t, \theta_C) e^{jm 2\pi d \sin(\theta)/\lambda}, \quad (10)$$

where  $s_m(t, \theta_C)$  is taken from (9) and the exponential term is the delay resulting from path length differences as a function of angle  $\theta$ . Note that the dependence on the waveform code  $\mathbf{x}_w$  and spatial modulation code  $\mathbf{x}_s$  have been suppressed for the sake of compact representation. If the set of  $M$  waveforms  $s_m(t, \theta_C)$  are identical aside from a scalar phase shift (no spatial modulation applied) then the emission  $g(t, \theta, \theta_C)$  is just the original waveform  $s(t)$  beamformed in the direction  $\theta_C$ , i.e. the temporal modulation is decoupled from the spatial angle. Otherwise, however, a different temporal waveform will be observed at different spatial angles  $\theta$  in the far-field.

Using (10), the instantaneous spatial features generated with the WDA can be examined using the time-varying beampattern (TVBP) denoted as

$$B_{TV}(t, \theta, \theta_C) = g(t, \theta, \theta_C) g^*(t, \theta, \theta_C) \quad (11)$$

for  $0 \leq t \leq T$ , where  $(\bullet)^*$  denotes complex conjugation. Integrating (11) over the pulse width and dividing by  $T$  yields the aggregate beampattern

$$B(\theta, \theta_C) = \frac{1}{T} \int_0^T g(t, \theta, \theta_C) g^*(t, \theta, \theta_C) dt. \quad (12)$$

As discussed above, if no spatial modulation is present the product  $g(t, \theta, \theta_C) g^*(t, \theta, \theta_C)$  is a constant over the pulse width such that  $B(\theta, \theta_C)$  yields the usual *array factor* beampattern [26] steered to  $\theta_C$ .

On receive (and assuming negligible Doppler shift of the resulting echoes during the pulsewidth), the reflected signal incident upon the  $m^{\text{th}}$  indexed antenna element can be expressed as

$$y_m(t, \theta_C) = \int \left[ x(t, \theta) * g(t, \theta, \theta_C) e^{jm 2\pi d \sin(\theta)/\lambda} \right] d\theta + u(t), \quad (13)$$

where  $x(t, \theta)$  is the complex scattering as a function of time (delay) and spatial angle,  $u(t)$  is additive noise, and  $*$  represents convolution. Receive beamforming (in direction  $\beta$ ) and pulse compression can be performed as

$$z(t, \beta, \theta_C) = \frac{1}{M} \sum_{m=-(M-1)/2}^{(M-1)/2} y_m(t, \theta_C) e^{-jm 2\pi d \sin(\beta)/\lambda} \quad (14)$$

and

$$\hat{x}(\tau, \beta, \theta_C) = \int z(t, \beta, \theta_C) h^*(t - \tau, \beta, \theta_C) dt, \quad (15)$$

respectively, where  $h(t, \beta, \theta_C)$  is the pulse compression filter for receive angle  $\beta$  and  $\tau$  is the relative delay of the incident signal. The true matched filter for (15) would be  $h(t, \beta, \theta_C) = g(t, \beta, \theta_C)$ . However, because of the angle-delay coupling induced by spatial modulation it is useful to normalize the matched filter such that the gain is constant as a function of receive angle to avoid artificially scaling the estimated scattering response and the noise. As such, we define a unity-gain normalized matched filter as

$$h(t, \beta, \theta_C) = \frac{g(t, \beta, \theta_C)}{\left[ \int_0^T g(t, \beta, \theta_C) g^*(t, \beta, \theta_C) dt \right]^{1/2}} \quad (16)$$

so that (15) actually provides the matched filter estimate of the illumination-scaled response

$$\bar{x}(\tau, \beta, \theta_C) = x(\tau, \beta, \theta_C) \left[ \int_0^T g(t, \beta, \theta_C) g^*(t, \beta, \theta_C) dt \right]^{1/2}. \quad (17)$$

Using the coherent receive processing defined in (14)-(16), an angle-delay ambiguity function (ADAF) can be constructed as

$$A(\tau, \theta, \beta, \theta_C) = \left| \frac{\int_0^T \left[ \sum_{m=-(M-1)/2}^{(M-1)/2} g(t, \theta, \theta_C) e^{jm\bar{\theta}} g^*(t-\tau, \beta, \theta_C) e^{-jm\bar{\beta}} \right] dt}{M \left[ \int_0^T g(t, \beta, \theta_C) g^*(t, \beta, \theta_C) dt \right]^{1/2}} \right|^2 \quad (18)$$

where the electrical angle corresponding to a signal arriving from spatial angle  $\theta$  is

$$\bar{\theta} = \frac{2\pi d}{\lambda} \sin(\theta), \quad (19)$$

and the electrical angle corresponding to the receive filter tuned to spatial angle  $\beta$  is

$$\bar{\beta} = \frac{2\pi d}{\lambda} \sin(\beta). \quad (20)$$

Note that due to the normalization factors in (7), (10), (14), and (16), the case of standard beamforming (no spatial modulation) realizes a response for (18) at  $\tau = 0$  and  $\beta = \theta$  that achieves the maximum value of unity. Thus the “beam smearing” loss of spatial modulation can be directly determined. Also, while not considered here, Doppler can be readily incorporated into (18) to obtain an angle-delay-Doppler ambiguity function. Finally, as long as the array narrowband assumption holds, this emission and subsequent analysis framework can be easily modified for arbitrary array structures.

### C. WDA Spectral Impact

The spatial modulation in (7) also produces a convolution in frequency that serves to expand the bandwidth relative to standard beamforming (using the same waveform). The emissions from the outer elements of the array, having the largest indices of  $m = \pm(M-1)/2$  in (8), thus exhibit the largest additional spectral excursion from the carrier frequency. Here we examine the degree of bandwidth expansion for the illustrative example of a linear frequency modulated (LFM) waveform and linearly scanning spatial modulation, where the latter subsumes the frequency diverse array framework [5-12] for a pulsed emission. This example then permits the statement of a general bandwidth expansion expression.

Relative to the center direction  $\theta_C$ , with associated electrical angle  $\bar{\theta}_C$  via (19), consider the spatial deviation over the interval corresponding to the first nulls in either direction. Define  $\Delta_{\text{null},+}$  and  $\Delta_{\text{null},-}$  as the positive and negative spatial angle deviations corresponding to the first nulls that respectively realize the electrical angles

$$\begin{aligned}\bar{\theta}_{\text{null},+} &= \frac{2\pi d}{\lambda} \sin(\theta_C + \Delta_{\text{null},+}) \\ \bar{\theta}_{\text{null},-} &= \frac{2\pi d}{\lambda} \sin(\theta_C + \Delta_{\text{null},-})\end{aligned}\quad (21)$$

For  $M$  antenna elements with inter-element separation  $d$  the electrical angle phase change that results from traversing from one first-null to the other is proportional to  $2\lambda/Md$  [26] as

$$\begin{aligned}|\bar{\theta}_{\text{null},+} - \bar{\theta}_{\text{null},-}| &= \left(\frac{2\pi d}{\lambda}\right) |\sin(\theta_C + \Delta_{\text{null},+}) - \sin(\theta_C + \Delta_{\text{null},-})| = \left(\frac{2\pi d}{\lambda}\right) \frac{2\lambda}{Md} \\ &= \frac{4\pi}{M}\end{aligned}\quad (22)$$

Generalizing (22) to the traversal of  $K$  null-to-null intervals thus realizes an electrical angle phase change of  $4\pi K/M$ , where  $0 \leq K \leq M/2$  (and  $K$  need not be an integer) with the upper limit corresponding to a boresight center direction with spatial traversal from one endfire direction to the other during the pulse. From an “energy on target” perspective and in light of the small perturbations observed for fixational eye movement [16-18], it seems likely that one would wish  $K$  to be relatively small (perhaps  $\leq 1$ ).

Using (4) and (8), the outermost elements scale the electrical angle phase change by the largest value of  $(M-1)/2$  so that, based on (22), the total electrical angle phase change at these elements when traversing  $K$  null-to-null spatial intervals is

$$\text{outer elements phase change} = \pm K \left( \frac{4\pi}{M} \right) \left( \frac{M-1}{2} \right) \cong \pm 2\pi K \quad (23)$$

for  $M$  sufficiently large. For the case of linear spatial modulation over the pulsewidth and under the assumption that  $K$  and  $\theta_C$  are such that a linear spatial angle traversal corresponds sufficiently well to a linear electrical angle phase change, then at the outer antenna elements the spatial modulation induces a frequency shift upon the underlying waveform  $s(t; \mathbf{x}_w)$  in the amount of

$$\text{outer element frequency shift} \cong \frac{\pm 2\pi K}{T} = \frac{\pm 2\pi K/N}{T_p}, \quad (24)$$

where we have used the relationship  $T = NT_p$  defined for the CPM implementation. The numerator in (24) corresponds to the  $m\varepsilon_n$  term in (9) when  $m = \pm(M-1)/2$  so that

$$\varepsilon_n = \frac{2\pi K}{N} \div \left( \frac{M-1}{2} \right) = \frac{4\pi K}{N(M-1)}. \quad (25)$$

As demonstrated in (25) for linear spatial modulation,  $\varepsilon_n$  is a constant as a function of time index  $n$ . It is important to note, however, that for a linear frequency modulated (LFM) waveform implemented with CPM, the values of  $\alpha_n$  exhibit a uniform sampling on the interval  $[-\pi, \pi]$  as a function of  $n$  [27,28]. Furthermore, as defined by the structure of the CPM implementation in (1)-(3), the maximum phase changes over the transition interval  $T_p$  are  $\pm\pi$  for the LFM waveform. These limits on the phase change were defined in [21] to aid in spectral containment but there is no physical or mathematical reason why they cannot be exceeded (see [29] for further discussion of this “over-coding” effect).

Combining the waveform and spatial modulations as  $(\alpha_n - m\varepsilon_n)$  from (9) and using the maximum phase transitions for each via (25),  $m = \pm(M-1)/2$ , and  $\alpha_n = \pm\pi$ , we find that the maximum total instantaneous phase changes over the transition interval  $T_p$ , which otherwise establish the outermost frequency components of the emission (therefore demarcating the bandwidth), are thus

$$\text{outermost frequencies} = \frac{\pm(2\pi K/N + \pi)}{T_p}. \quad (26)$$

In other words, relative to traditional beamforming, linear spatial modulation of an LFM waveform involves a bandwidth increase by a factor of

$$\text{(linear) bandwidth increase factor} = \frac{2 \times (2\pi K/N + \pi)}{2\pi} = 1 + 2K/N, \quad (27)$$

where the leading 2 in the numerator and denominator arises from the  $\pm$  attribute of (26) and the phase-change support of  $\alpha_n \in [-\pi, \pi]$  for LFM implemented using CPM.

In general for an arbitrary waveform and spatial modulation implemented using (9), the total bandwidth increase can be expressed as

$$\begin{aligned} \text{(general) bandwidth increase factor} = \\ \frac{\max\{\alpha_n \pm \varepsilon_n (M-1)/2\} - \min\{\alpha_n \pm \varepsilon_n (M-1)/2\}}{\max\{\alpha_n\} - \min\{\alpha_n\}} \end{aligned} \quad (28)$$

where  $\varepsilon_n$  need not be a constant (i.e. can be nonlinear spatial modulation). The bandwidth metric in (28) also implies that joint optimization of the waveform and spatial modulations via selection of  $\alpha_n$  and  $\varepsilon_n$  for  $n=1, \dots, N$  may be performed in such a way as to bound the total bandwidth by establishing a constraint relationship between each of the  $[\alpha_n, \varepsilon_n]$  pairs.

#### D. WDA Emission Evaluation

To demonstrate the attributes of this spatially-modulated emission scheme, we employ the CPM implementation (via (3)) of a length  $N = 200$  code  $\mathbf{x}_w$  to produce a LFM waveform (CPM very closely approximates LFM akin to a first-order hold representation using linear phase segments that can be made arbitrarily small). The antenna array is a  $M = 30$  element uniform linear array with half-wavelength element spacing and with  $\theta_C = 0^\circ$  (i.e. boresight center direction). Thus null-to-null spatial scanning ( $K = 1$ ) comprises  $\pm 3.8^\circ$  in spatial angle. The pulsewidth is set to  $T = 1$  for convenience of illustration.

Using this known waveform we consider four cases of spatial modulation. In Case 1 standard stationary beamforming is used to provide a baseline for comparison. In contrast, Case 2 employs spatial

modulation over the pulsewidth and scans linearly from 1<sup>st</sup> null to 1<sup>st</sup> null (on each side). Likewise, Case 3 uses linear spatial scanning, albeit from 2<sup>nd</sup> null to 2<sup>nd</sup> null relative to  $\theta_C=0^\circ$  (so  $K=2$ ). Finally, Case 4 considers spatial modulation involving a half cycle of a sinusoid that is likewise centered on  $\theta_C=0^\circ$  and with maximum spatial excursions of the 1<sup>st</sup> nulls occurring at the beginning and end of the pulse.

Figure 3 illustrates the time-varying beampattern from (11) for each of the four cases. As one would expect from an instantaneous perspective, the spatial mainbeam and sidelobes retain the same structure across the four cases, albeit tilted or twisted according to the spatial modulation structure. When the beampattern is considered in aggregate over the pulsewidth, the spatial modulation has the effect of “smearing” the beam as shown in Fig. 4 resulting in an aggregate mainbeam that is lower and wider than that of the standard beamforming case. Clearly a peak SNR penalty results at  $\theta_C$  from using spatial modulation. However, in contrast to what the aggregate beampattern appears to indicate, spatial modulation can in fact enhance spatial resolution due to angle-delay coupling.

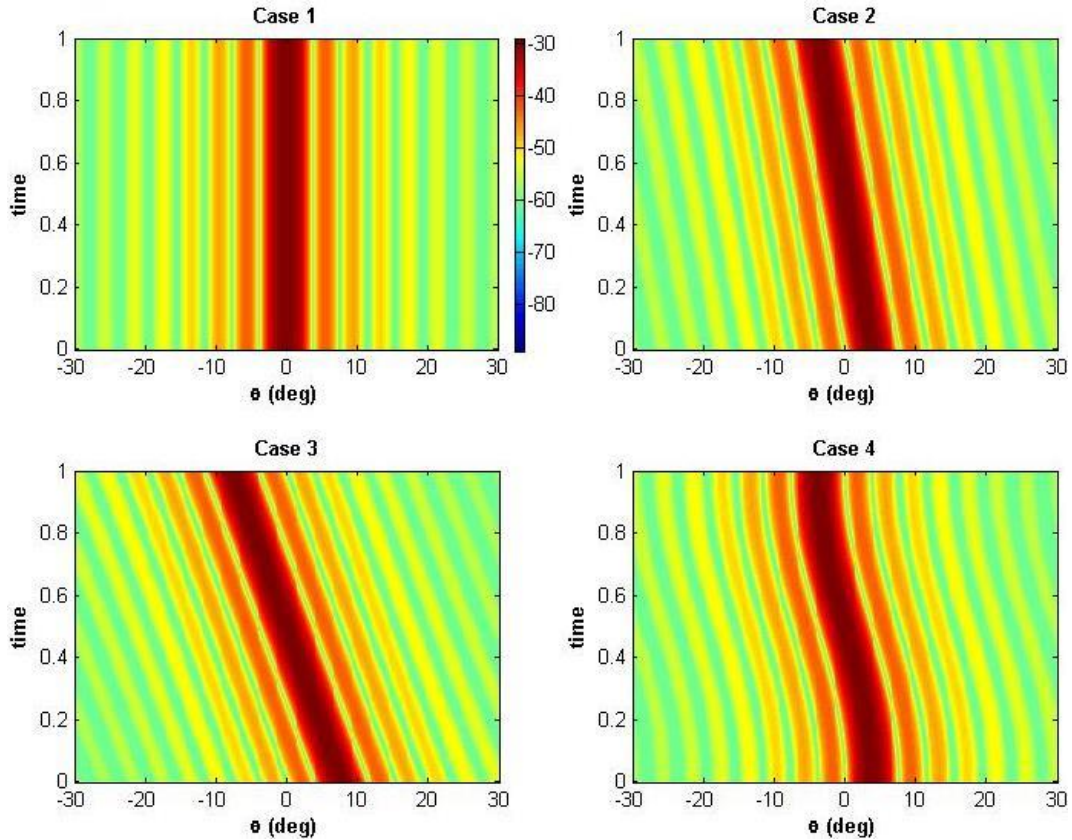


**Figure 3** Time-varying beam pattern (TVBP) for Case 1) standard beamforming, Case 2) null-to-null linear spatial modulation, Case 3) double null-to-null linear spatial modulation, and Case 4) null-to-null half-cycle sinusoidal spatial modulation

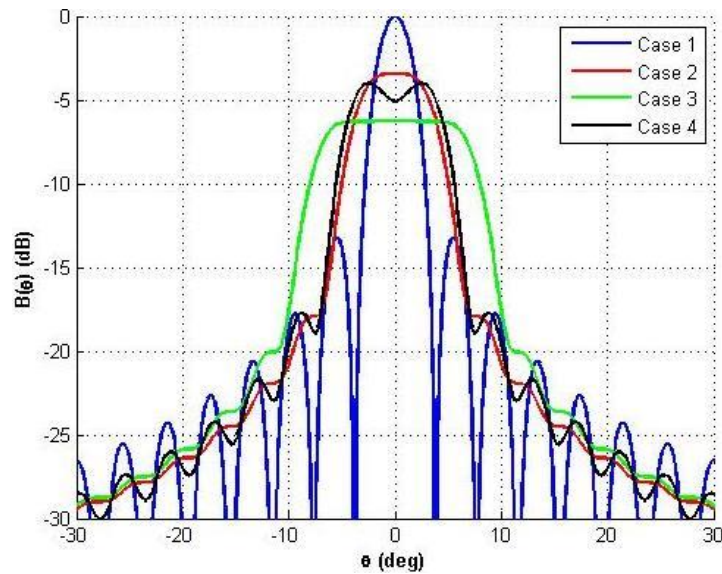


**Figure 4** Aggregate beam pattern for Case 1) standard beamforming, Case 2) null-to-null linear spatial modulation, Case 3) double null-to-null linear spatial modulation, and Case 4) null-to-null half-cycle sinusoidal spatial modulation

To examine the impact of delay-angle coupling it is instructive to consider various cuts of the ambiguity function in (18). Figure 5 depicts the delay matched point ( $\tau=0$ ) for the four emission schemes as a function of transmit angle  $\theta$  and receive angle  $\beta$ . Here it is observed that relative to standard beamforming (Case 1) the spatial modulation Cases 2-4 exhibit a mainbeam that is elongated along the  $\theta = \beta$  axis while the sidelobes not on this axis are markedly lower. In other words, for transmit angles  $\theta$  that are different from a given receive angle  $\beta$ , spatial modulation can result in a lower cross-correlation of the associated angle-dependent waveforms.

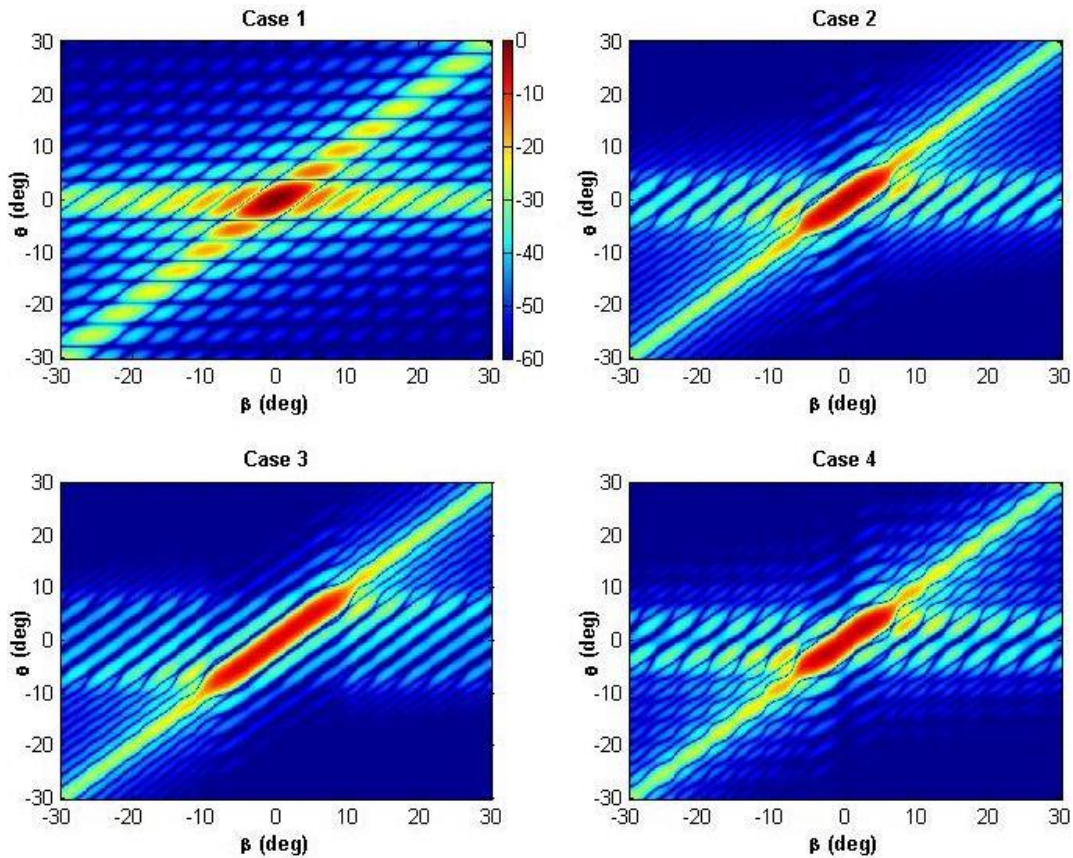


**Figure 5**  $\tau = 0$  cut of angle-delay ambiguity function for Case 1) standard beamforming, Case 2) null-to-null linear spatial modulation, Case 3) double null-to-null linear spatial modulation, and Case 4) null-to-null half-cycle sinusoidal spatial modulation

Taking the  $\theta = 0^\circ$  cut of the responses in Fig. 5 and peak-normalizing for easy comparison yields the results shown in Figs. 6 and 7. In Fig. 6 we find that, relative to the peak, the sidelobes of the three spatial

modulation emissions are at least 5 dB lower than the standard beamforming case. Furthermore, Fig. 7 shows that the mainbeam is in fact narrower for the three spatial modulation cases. Specifically, when measured 3 dB down from the peak Cases 2, 3, and 4 realize spatial resolution enhancement relative to standard beamforming of 23%, 27%, and 30%, respectively. In other words, delay-angle coupling reduces the ambiguity between different spatial angles via lower spatial sidelobes and enhanced spatial resolution at the expense of reduced “energy on target” in a specific direction as illustrated by the aggregate beam pattern. Under conditions of adequate stationarity for the illuminated region [25], more pulses may be used (relative to the standard case) to compensate for this loss while retaining the same spatial coverage.

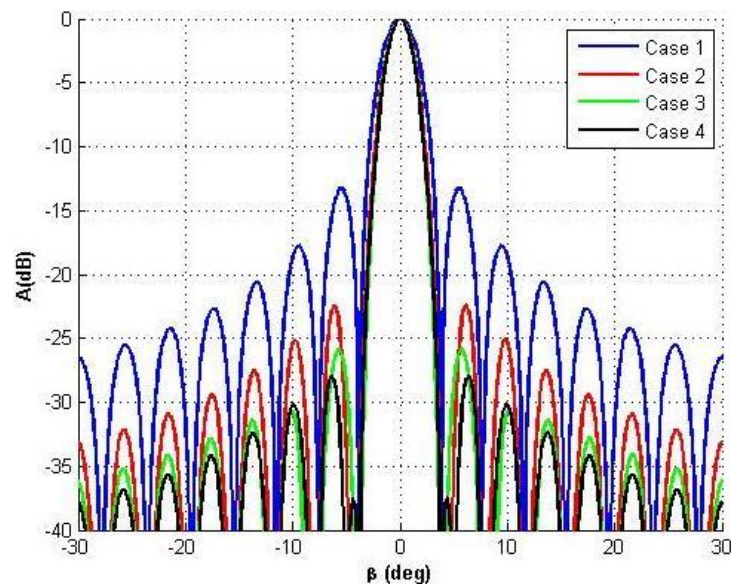


**Figure 6** Peak-normalized  $\tau = 0$ ,  $\theta = 0^\circ$  cut of angle-delay ambiguity function for Case 1) standard beamforming, Case 2) null-to-null linear spatial modulation, Case 3) double null-to-null linear spatial modulation, and Case 4) null-to-null half-cycle sinusoidal spatial modulation

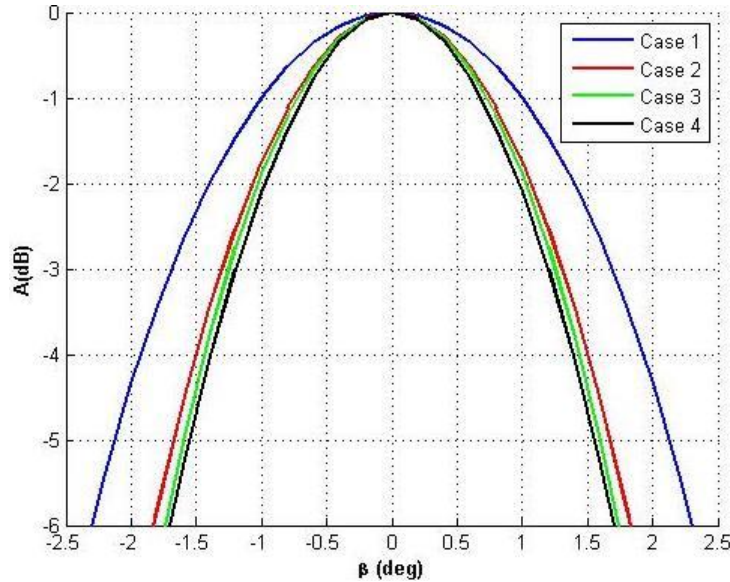


**Figure 7** Peak-normalized  $\tau = 0$ ,  $\theta = 0^\circ$  cut of angle-delay ambiguity function (mainbeam close-up) for Case 1) standard beamforming, Case 2) null-to-null linear spatial modulation, Case 3) double null-to-null linear spatial modulation, and Case 4) null-to-null half-cycle sinusoidal spatial modulation

It is also instructive to consider the angle-delay ambiguity as a function of  $\tau$  and  $\beta$  for the  $\theta = 0^\circ$  cut (Fig. 8) where it is interesting to note the lack of observable range sidelobes for the spatial modulation cases (2-4). It is important to point out, however, that this result is specific to the particular waveform and spatial modulations shown here and would differ for various waveform/spatial modulation combinations. If we select the  $\beta = 0^\circ$  cut of the response in Fig. 8 for closer inspection, the delay dimension can be isolated as shown in Fig. 9. Of the four, standard beamforming (Case 1) clearly exhibits the best range resolution. That said, the spatial modulation schemes examined here realize orders-of-magnitude lower range sidelobes at the expense of some degradation in range resolution (and peak power as previously indicated). These cases produce an effect akin to waveform amplitude tapering, albeit with this effect being produced by spatial modulation in the far field as opposed to actual amplitude weighting in the transmitter that would otherwise preclude the operation of power amplifiers in saturation.

Note that not all means of spatial modulation necessarily provide a range sidelobe improvement. It was shown in [1] that a full-cycle sinusoid produced very high near-in range sidelobes. This effect could be the result of re-traversing the same spatial angles in the second half of the sinusoidal cycle so that the range-angle ambiguity is dominated by the cross-correlation of the associated waveform segments that

share the same spatial angles. Thus if spatial modulation is to be used, the joint waveform/spatial modulation structure must be considered.

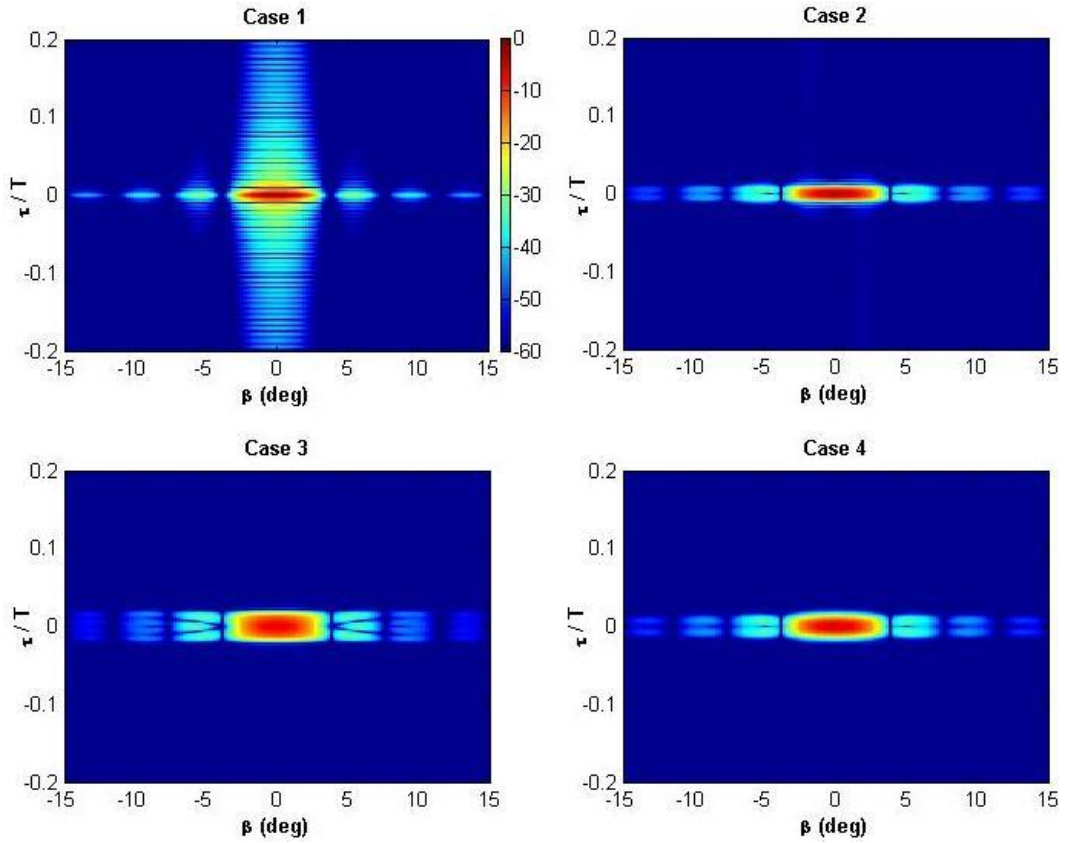


**Figure 8**  $\theta = 0^\circ$  cut of angle-delay ambiguity function for Case 1) standard beamforming, Case 2) null-to-null linear spatial modulation, Case 3) double null-to-null linear spatial modulation, and Case 4) null-to-null half-cycle sinusoidal spatial modulation

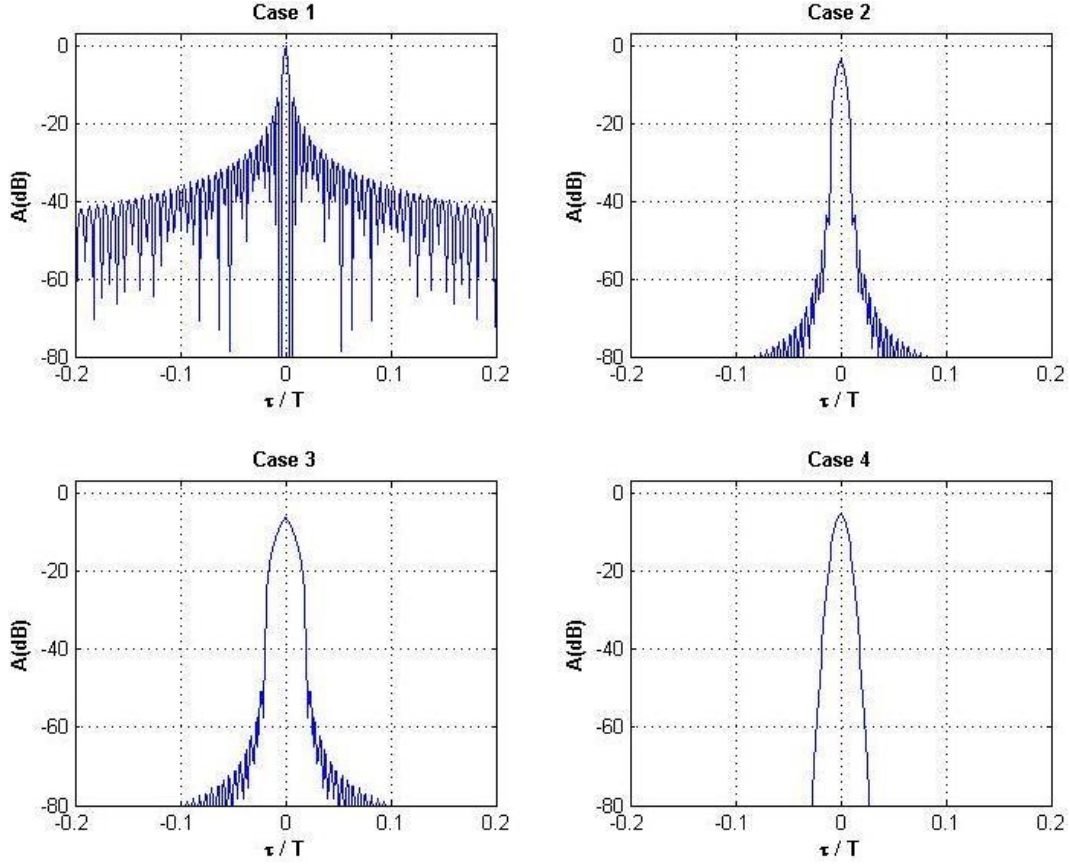


**Figure 9**  $\theta = 0^\circ$ ,  $\beta = 0^\circ$  cut of angle-delay ambiguity function for Case 1) standard beamforming, Case 2) null-to-null linear spatial modulation, Case 3) double null-to-null linear spatial modulation, and Case 4) null-to-null half-cycle sinusoidal spatial modulation

Finally, Figs. 10-13 depict spectral content (normalized by pulsewidth  $T$ ) for the four cases. For Case 1 (Fig. 10) the same waveform is emitted by every antenna element so only the single spectral plot is shown for baseline comparison. For Cases 2-4 the spectral content is depicted in Figs. 11-13 for the emissions from the outermost elements of the length  $M = 30$  uniform linear array along with a center-most element emission for comparison, which by the enforced symmetry will experience negligible effects from spatial modulation for the cases considered. For the ease of the reader, the elements are labeled from left-to-right as  $1, 2, \dots, 30$  with element 15 used as the center-most element. In terms of the position indexing previously defined, the elements shown are indices  $m = -0.5(29) = -14.5$  (1<sup>st</sup> element),  $m = -0.5(29) + 14 = -0.5$  (15<sup>th</sup> element), and  $m = -0.5(29) + 29 = +14.5$  (30<sup>th</sup> element).

The LFM waveform implemented here with CPM is constructed from a  $N = 200$  code [21] thus yielding a time-bandwidth product of  $BT \cong 200$  as evidenced by the pulsewidth-normalized 3 dB

bandwidth for the standard beamforming case in Fig. 10. Defining an *aggregated bandwidth* as that established by the 3 dB collective bandwidths demarcated by the outermost element emissions, it is found in Fig. 11 that the normalized aggregated bandwidth for the null-to-null linear spatial modulation of Case 2 is 202, a 1% increase over standard beamforming which agrees with (27). Likewise, the (Case 3) double null-to-null linear spatial modulation result in Fig. 12 realizes a normalized aggregated bandwidth of 204, a 2% increase as predicted by (27). For the half-cycle sinusoidal Case 4 we must use the more general (28). However, this case experiences negligible spatial modulation at the beginning and ends of the pulse (per examination of Fig. 3) where LFM yields the greatest excursions from the center frequency. Thus, as observed in Fig. 13, the half-cycle sinusoidal spatial modulation combined with an LFM waveform exhibits no bandwidth increase.

To demonstrate the utility of (28) consider the full-cycle sinusoid spatial modulation examined in [1] where the extremum values of  $(\alpha_n - m \varepsilon_n)$  are found to be  $\pm 3.237$  (in radians) thereby predicting a 3% increase in aggregated bandwidth. This prediction agrees with the result in Fig. 14 that depicts a normalized aggregated bandwidth of 206.

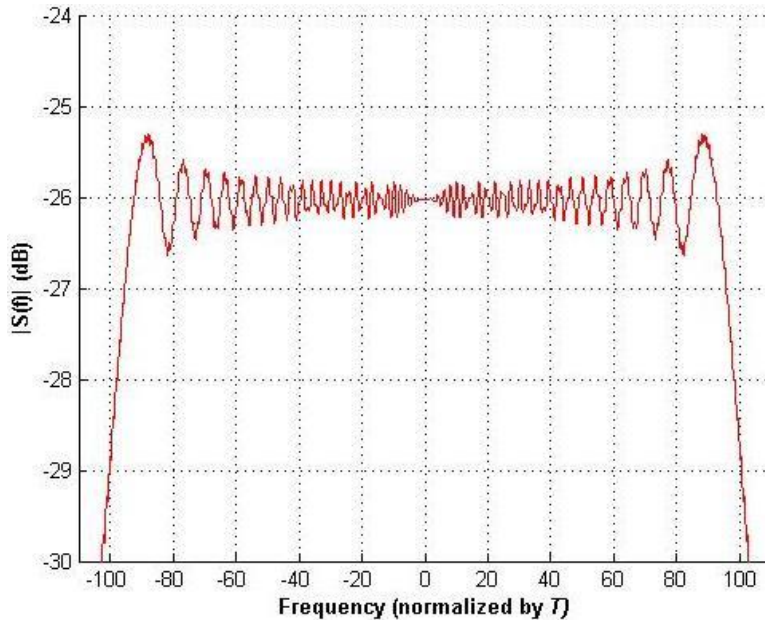


**Figure 10** Normalized spectral content for Case 1) standard beamforming – normalized bandwidth = 200 (baseline case)

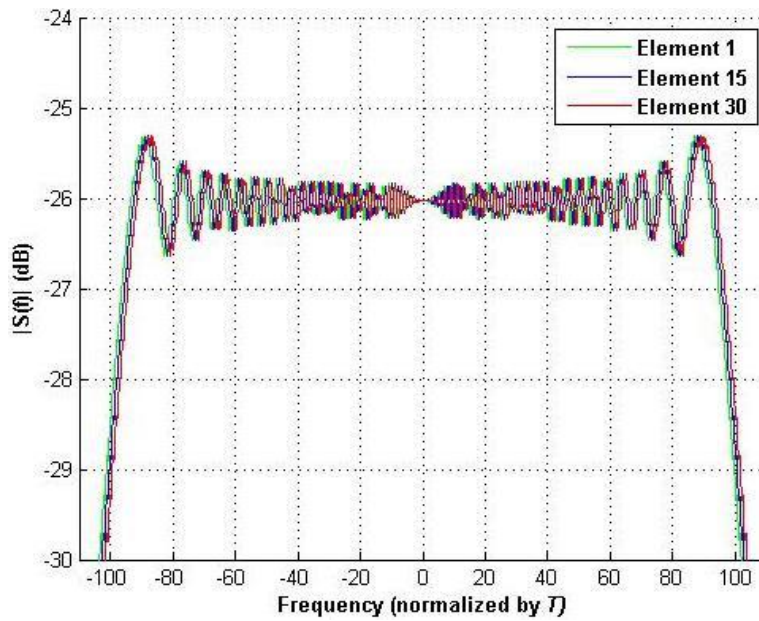


**Figure 11** Normalized spectral content for Case 2) null-to-null linear spatial modulation – aggregated normalized bandwidth = 202 (or 1% bandwidth increase)

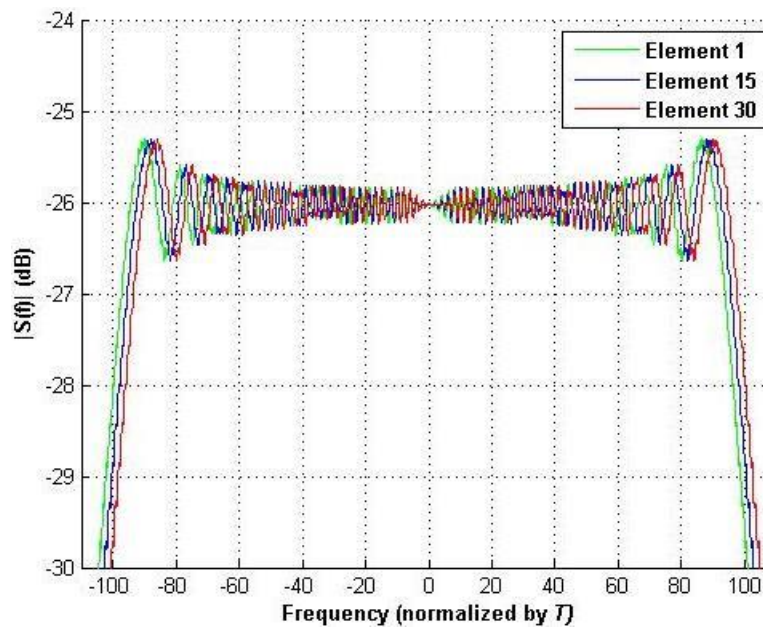


**Figure 12** Normalized spectral content for Case 3) double null-to-null linear spatial modulation – aggregated normalized bandwidth = 204 (or 2% bandwidth increase)

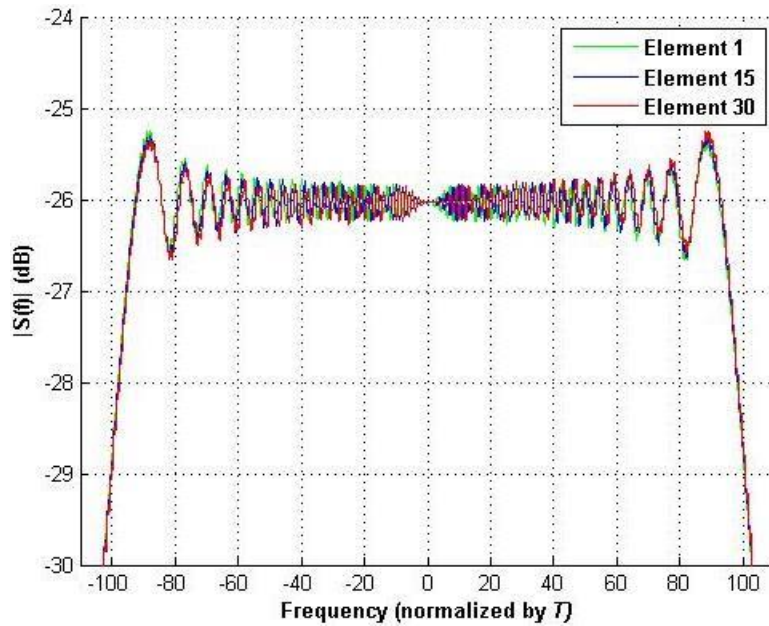


**Figure 13** Normalized spectral content for Case 4) null-to-null half-cycle sinusoidal spatial modulation – aggregated normalized bandwidth = 200 (so no bandwidth increase)

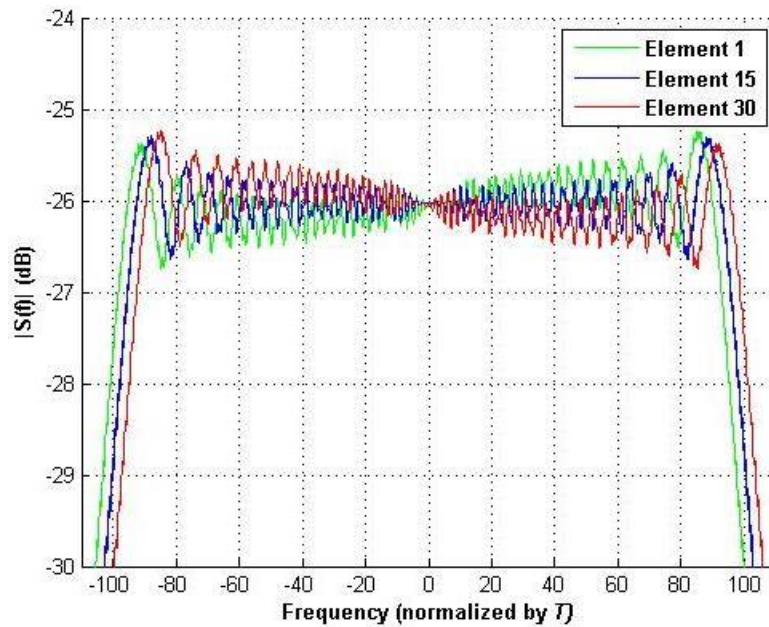


**Figure 14** Normalized spectral content for Case 4) null-to-null sinusoidal spatial modulation – aggregated normalized bandwidth = 206 (or 3% bandwidth increase)

These cases were selected to provide a snapshot of the diverse possible emission structures that may be achieved by combining spatial and waveform modulations. From a cognitive sensing perspective one can

envision the development of a set of underlying code pairs  $(\mathbf{x}_w, \mathbf{x}_s)$  that possess different degrees of range and spatial resolution and sidelobe characteristics. In fact, considering a tracking modality in which some prior knowledge may be presumed with regard to target number and range-angle dispositions within a local region based on previous state estimates, code pairs could potentially be defined that enhance, in a scenario-dependent manner, the range-angle discrimination of targets for enhanced tracking performance.

### III. SIMULATION RESULTS

In Section II.D the spatial modulation structure was assessed with regard to the characteristics of different joint delay-angle emission schemes. Here we consider these emission schemes in terms of the output of receive processing for a couple representative target scenarios. In the first scenario two targets are present at the same range with angular separation commensurate with the spatial resolution of standard beamforming. In the second scenario five targets are present that form a ‘X’ in range and angle to illustrate the impact of the different emission schemes in both dimensions. In both cases the targets possess a receive SNR that is 20 dB following coherent integration (based on individual standard beamforming for each target). The same emission parameterization as Section II.D is used so  $N = 200$  (which approximates the waveform time-bandwidth product) and the antenna is comprised of  $M = 30$  elements with half-wavelength spacing. For both scenarios the center direction is set to  $\theta_C = 0^\circ$  such that the first nulls are  $\pm 3.8^\circ$  in spatial angle.

Due to the pulsed nature of the radar, Nyquist receive sampling can only be approximated, though the good spectral containment of the CPM implementation [21] certainly helps to keep the “over-sampling” relative to the 3 dB bandwidth to a nominal level. For the results shown the receiver matched filtering is performed for a sampling rate that is three times that of the 3 dB waveform bandwidth. As such, a waveform generated from code length  $N = 200$  realizes a matched filter with a discretized length of 600.

### A. *Two Targets at Same Range*

Consider two targets occupying the same range (range index 200) and at spatial angles of  $\pm 2^\circ$  (roughly nominal resolution for  $M = 30$  element array). The targets are in-phase which is known to be the most difficult case for achieving separation using beamforming. Figure 15 shows the delay-angle response from beamforming and pulse compression as defined in (14)-(16) for the four spatial modulation schemes described in Fig. 3. For standard beamforming (Case 1) we only observe a single target centered in between the two true angles because the target angles correspond to the nominal resolution separation and are in-phase (thus inhibiting their separation). However, when the emission is the null-to-null linear spatial modulation of Case 2, we find that the two targets are now clearly visible. The double null-to-null linear modulated emission of Case 3 likewise realizes two separate targets, though SNR is noticeably reduced relative to Case 2 due to greater energy dispersal across spatial angle (unnecessarily in this case). Finally, Case 4 shows the response of the null-to-null half-cycle sinusoidal spatial modulation which appears to provide marginally the best overall performance of these four considered based on the shape and disposition of the matched filter response.

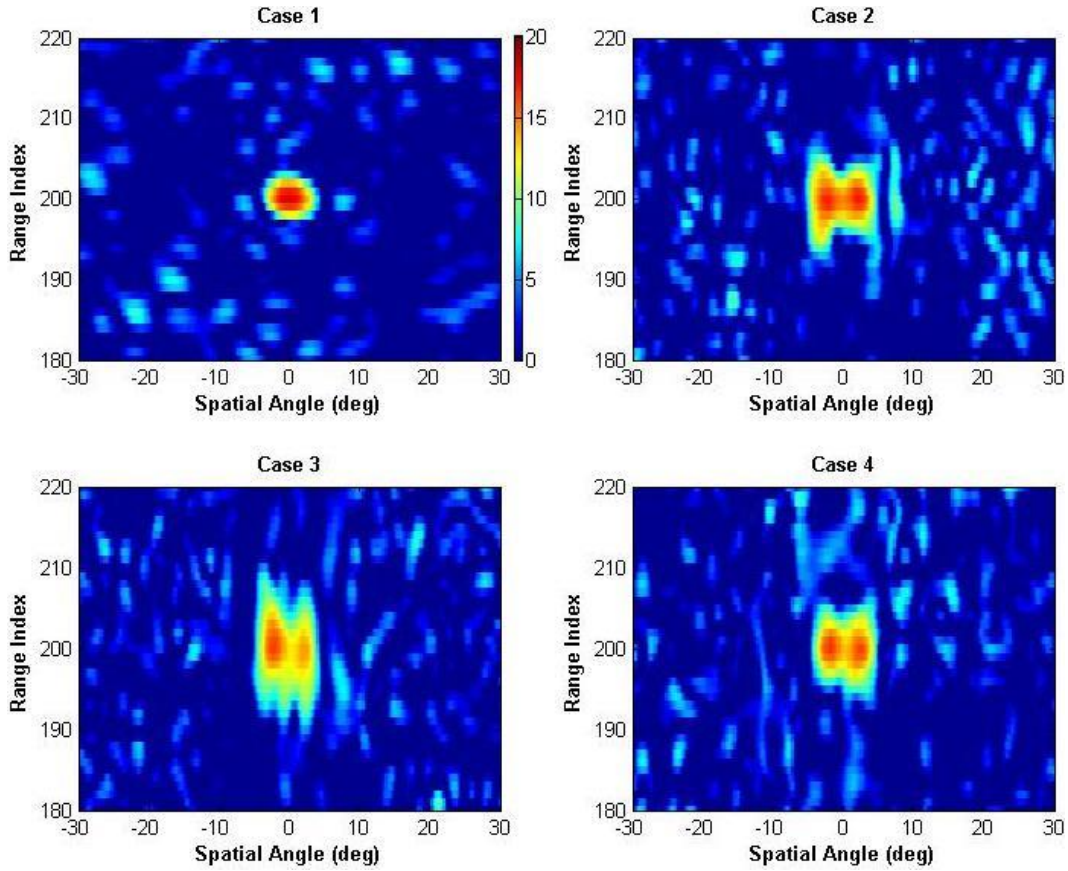


**Figure 15** Two-target scenario for Case 1) standard beamforming, Case 2) null-to-null linear spatial modulation, Case 3) double null-to-null linear spatial modulation, and Case 4) null-to-null half-cycle sinusoidal spatial modulation

### B. Five Targets in a Range-Angle ‘X’ Arrangement

Now consider five targets phase in an ‘X’ pattern where two of the targets occupy the same range (index 196) at spatial angles  $\pm 3^\circ$ , a center target resides at range index 200 at spatial angle  $0^\circ$ , and two more targets occupy range index 204 at spatial angles  $\pm 3^\circ$ . Each target phase is randomly assigned yet remains fixed for the four emission schemes considered to provide a fair comparison. Figure 16 reveals the results for this scenario. For standard beamforming (Case 1) the center target at  $0^\circ$  spatial angle is clearly shown, though the other four targets at different spatial angles are not visible aside from a smaller response that may be from the top-left target in the ‘X’. In contrast, the null-to-null linear spatial modulation (Case 2) does capture all five target echoes, though they are not necessarily distinguishable as separate. The double null-to-null linear spatial modulation (Case 3), on the other hand, exhibits greater

smearing than the previous linear case and reveals no evident response from the lower-left target. Finally, the half-cycle sinusoid spatial modulation (Case 4) appears to be quite similar to the linear emission of Case 2, which upon comparison of their fast-time beam trajectories from Fig. 3 is not unexpected.

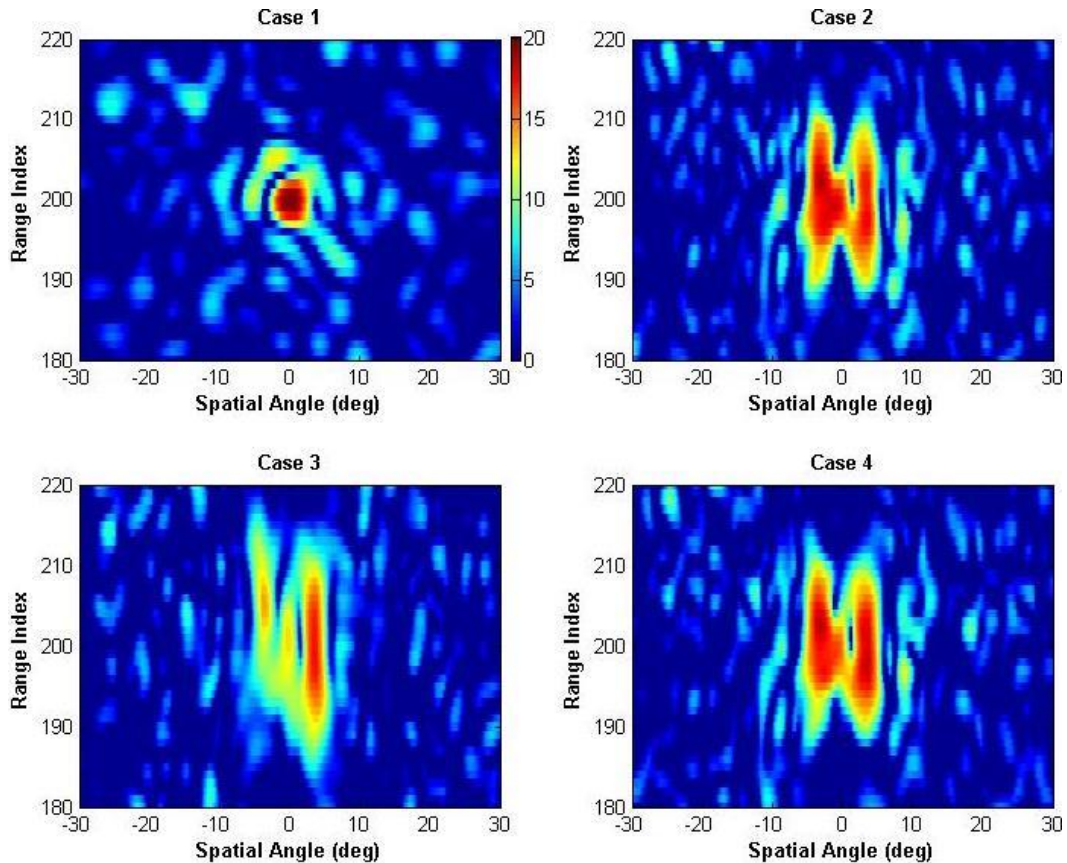


**Figure 16** Five-target ‘X’ scenario for Case 1) standard beamforming, Case 2) null-to-null linear spatial modulation, Case 3) double null-to-null linear spatial modulation, and Case 4) null-to-null half-cycle sinusoidal spatial modulation

It should be noted that the random phase relationship between the targets does have an effect on how well these closely-spaced targets can be identified, which is also dependent upon the spatial modulation scheme; thus the single instantiation depicted in Fig. 16 is an incomplete characterization. To provide a somewhat broader characterization and also to demonstrate how spatial modulation may exploit the phase diversity of multiple targets, consider the response from four consecutive pulses of each emission scheme upon the same five-target ‘X’ scenario under the condition that the target phases are likewise randomly

(and independently) assigned for each pulse. Note that this randomly varying phase condition is not meant to represent a particular operational radar mode or scenario but is simply being used as a generic example. Because no knowledge is presumed regarding the targets' pulse-to-pulse phase responses, non-coherent integration of the echoes from the four pulses is used to compare the four emission schemes.

Figure 17 illustrates the results of the four spatial modulation schemes after non-coherent integration over four pulses. Standard beamforming (Case 1) now realizes a "halo effect" surrounding the center target with an SNR of about 8 dB (compared to the 20 dB center target response). While this halo could be viewed as potentially indicative of surrounding targets, it is far from conclusive evidence. In stark contrast to standard beamforming the result for the linear spatial modulation of Case 2 now reveals all five targets, albeit with a shallow null between the leftmost top and bottom targets. The target resolvability is less prominent for the double linear (Case 3) and half-cycle sinusoid (Case 4) spatial modulations, yet all five target responses are still evident. Clearly, this enhancement would not have occurred if the relative target phases were coherent with one another from pulse to pulse, though that may be an extreme case depending upon the radar modality. However, it is anticipated that using a different spatial modulation scheme on each pulse followed by appropriate combining could provide even further benefit as a result of the additional diversity of pulse agility (and it would not rely upon phase diversity of the targets).

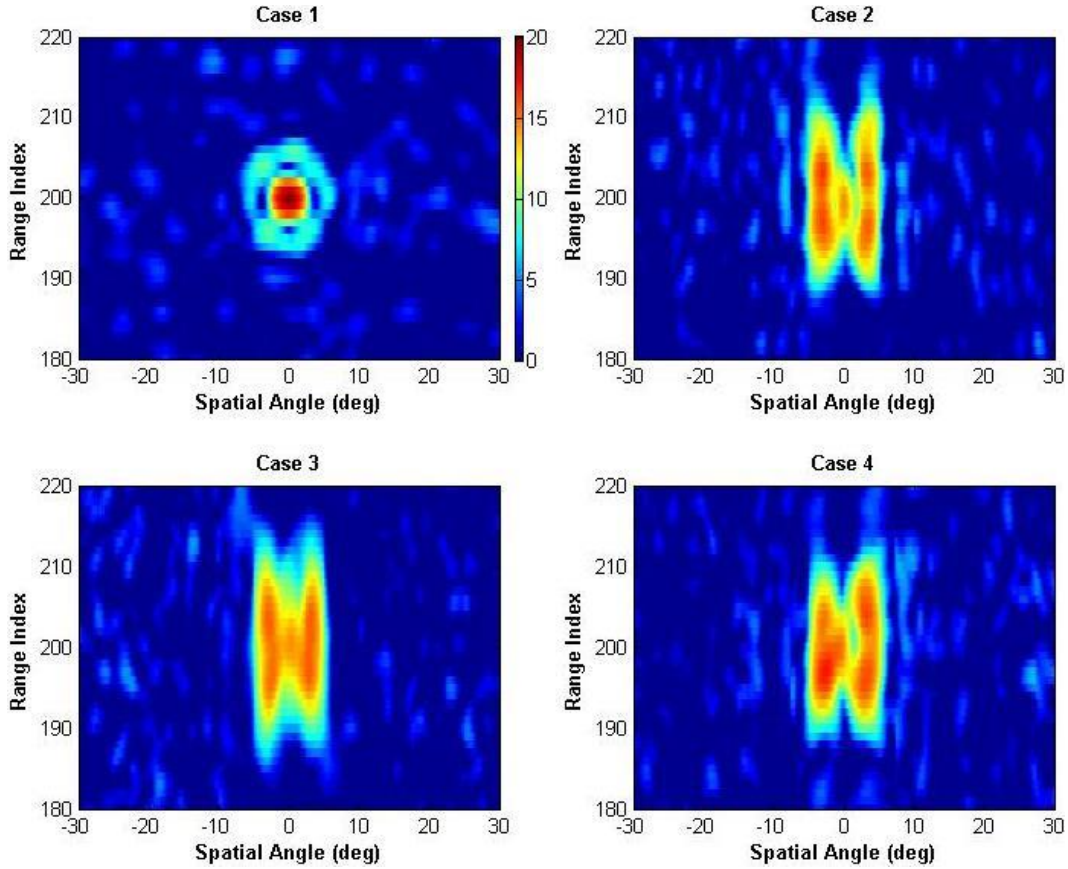


**Figure 17** Four-pulse non-coherent integration of five-target ‘X’ scenario for Case 1) standard beamforming, Case 2) null-to-null linear spatial modulation, Case 3) double null-to-null linear spatial modulation, and Case 4) null-to-null half-cycle sinusoidal spatial modulation

#### IV. CONCLUSIONS

Spatially modulating emissions during a pulse provides a form of MIMO radar that is consistent with the passive sensing paradigm of fixational eye movement found in nature. The resulting waveform-diverse array (WDA) concept presented here that is based on the continuous phase modulation (CPM) code-to-waveform implementation subsumes the frequency-diverse array concept for pulsed radar operation and also facilitates a general framework in which the joint delay-angle characteristics may be designed. A prospective application may be the incorporation of cognition into radar tracking, particularly of multiple proximate targets, by leveraging the operation of the visual cortex for an active sensing paradigm. It has been shown that different spatial modulation structures, when coupled with a standard LFM waveform, allow for different trade-offs in terms of resolution and sidelobe levels in both the delay and angle domains due to their inherent coupling. Further, the aggregate bandwidth over the collection of

emissions across the array is dependent on the relationship between the spatial and waveform modulations. Considering that the one-dimensional spatial array defined here can be readily extended to a two-dimensional planar array to enable spatial modulation in both azimuth and elevation and that the CPM implementation permits the implementation of arbitrary polyphase codes as transmitter-amenable waveforms, this joint (now delay-azimuth-elevation) emission structure establishes a very rich design space in which to explore new physically-realizable MIMO emission schemes. Ongoing work is exploring how the diversity afforded by this delay-angle coupling can be exploited to enhance target discrimination within a coherent processing interval of multiple pulses, how pulse agility may be incorporated, and how the development of a set of such waveform/spatial modulation emission pairs may be used for “on-the-fly” interrogation within a cognitive radar context.

### References

- [1] Blunt, S.D., McCormick, P., Higgins, T., Rangaswamy, M., “Spatially-modulated radar waveforms inspired by fixational eye movement,” *IEEE Radar Conference*, Cincinnati, OH, 19-23 May 2014.
- [2] Stoica, P. Li, J., Xie, Y. “On probing signal design for MIMO radar,” *IEEE Trans. Signal Processing*, vol. 55, pp. 4151-4161, Jan. 2008.
- [3] Fuhrmann, D., Browning, J.P., Rangaswamy, M., “Constant-modulus partially correlated signal design for uniform linear and rectangular MIMO radar arrays,” *Intl. Waveform Diversity and Design Conf.*, Orlando, FL, 9-13 Feb. 2009.
- [4] Fuhrmann, D., San Antonio, G., “Transmit beamforming for MIMO radar systems using signal cross correlations,” *IEEE Trans. Aerospace & Electronic Systems*, vol. 44, pp. 171-186, Jan. 2008.
- [5] Antonik, P., Wicks, M.C., Griffiths, H.D., Baker, C.J., “Range-dependent beamforming using element level waveform diversity,” *Intl. Waveform Diversity and Design Conf.*, Lihue, HI, 22-27 Jan. 2006.
- [6] Baizert, P., Hale, T.B., Temple, M.A., Wicks, M.C., “Forward-looking radar GMTI benefits using a linear frequency diverse array,” *IEE Electronics Letters*, vol. 42, pp. 1311-1312, Oct. 2006.
- [7] Secmen, M., Demir, S., Hizal, A., Eker, T., “Frequency diverse array antenna with periodic time modulated pattern in range and angle,” *IEEE Radar Conf.*, Waltham, MA, 17-20 Apr. 2007.
- [8] Higgins, T., Blunt, S.D., “Analysis of range-angle coupled beamforming with frequency-diverse chirps,” *Intl. Waveform Diversity & Design Conf.*, Orlando, FL, pp. 140-144, 8-13 Feb. 2009.
- [9] Sammartino, P.F., Baker, C.J., Griffiths, H.D., “Frequency diverse MIMO techniques for radar,” *IEEE Trans. Aerospace & Electronic Systems*, vol. 49, no. 1, pp. 201-222, Jan. 2013.
- [10] Wang, W.-Q., “Phased-MIMO radar with frequency diversity for range-dependent beamforming,” *IEEE Sensors Journal*, vol. 13, no. 4, pp. 1320-1328, Apr. 2013.
- [11] Duly, A.J., Love, D.J., Krogmeier, J.V., “Time-division beamforming for MIMO radar waveform design,” *IEEE Trans. Aerospace & Electronic Systems*, vol. 49, no. 2, pp. 1210-1223, Apr. 2013.
- [12] Antonik, P., Wicks, M.C., Griffiths, H.D., Baker, C. J., “Multi-mission multi-mode waveform diversity,” *IEEE Radar Conf.*, Verona, NY, 24-27 Apr. 2006.

- [13] Goodman, N.A., Stiles, J.M., "Resolution and synthetic aperture characterization of sparse radar arrays," *IEEE Trans. Aerospace & Electronic Systems*, vol. 39, no. 3, pp. 921-935, July 2003.
- [14] Stiles, J., Sinha, V., Nanda, A.P., "Space-time transmit signal construction for multi-mode radar," *IEEE Radar Conf.*, Verona, NY, 24-27 Apr. 2006.
- [15] Kapfer, R.M., Davis, M.E., "Ultra wideband, multi-mode radar processing," *IEEE Radar Conf.*, Atlanta, GA, pp. 95-100, 7-11 May 2012.
- [16] Rolfs, M., "Microsaccades: small steps on a long way," *Vision Research*, vol. 49, pp. 2415-2441, 2009.
- [17] Ahissar, E., Arieli, A., "Seeing via miniature eye movements: a dynamic hypothesis for vision," *Frontiers in Computational Neuroscience*, vol. 6, no. 89, Nov. 2012.
- [18] Cui, J., Wilke, M., Logothetis, N.K., Leopold, D.A., Liang, H., "Visibility states modulate microsaccade rate and direction," *Vision Research*, vol. 49, pp. 228-236, 2009.
- [19] Haykin, S., Xue, Y., Setoodeh, P., "Cognitive radar: step toward bridging the gap between neuroscience and engineering," *Proc. IEEE*, vol. 100, no. 11, pp. 3102-3130, Nov. 2012.
- [20] Jakobosky, J., Anglin, P., Cook, M., Blunt, S.D., Stiles, J., "Non-linear FM waveform design using marginal Fisher's information within the CPM framework," *IEEE Radar Conf.*, Kansas City, MO, 23-27 May 2011.
- [21] Blunt, S.D., Cook, M., Jakobosky, J., de Graaf, J., Perrins, E., "Polyphase-coded FM (PCFM) waveforms: part I: implementation," *IEEE Trans. Aerospace & Electronic Systems*, vol. 50, no. 3, pp. 2219-2230, July 2014.
- [22] *IRIG Standard 106-00: Telemetry Standards*, Range Commanders Council Telemetry Group, Range Commanders Council, White Sands Missile Range, New Mexico.
- [23] *Bandwidth-Efficient Modulations: Summary of Definitions, Implementation, and Performance*, Report Concerning Space Data System Standards, Informational Report CCSDS 413.0-G-2.
- [24] *Specifications of the Bluetooth System*, Bluetooth Special Interest Group, ver. 1.2, Nov. 2003.
- [25] Daum, F., Huang, J., "MIMO radar: snake oil or good idea?" *IEEE Aerospace and Electronic Systems Magazine*, vol. 24, no. 5, pp. 8-12, May 2009.
- [26] Van Trees, H.L., *Optimum Array Processing*, John Wiley & Sons, 2002, Chap. 2.
- [27] Jakobosky, J., Blunt, S.D., Cook, M.R., Stiles, J., Seguin, S.A., "Transmitter-in-the-loop optimization of physical radar emissions," *IEEE Radar Conf.*, Atlanta, GA, 7-11 May 2012.
- [28] Blunt, S.D., Cook, M., Jakobosky, J., de Graaf, J., Perrins, E., "Polyphase-coded FM (PCFM) waveforms: part II: optimization," *IEEE Trans. Aerospace & Electronic Systems*, vol. 50, no. 3, pp. 2231-2242, July 2014.
- [29] Jakobosky, J., Blunt, S.D., Himed, B., "Optimization of "over-coded" radar waveforms," *IEEE Radar Conference*, Cincinnati, OH, 19-23 May 2014.